Relativistic and semi-theoretical calculations of K-shell to L-shell/subshell vacancy transfer probabilities

Boualem Berkani[1,2], Abdelhalim Kahoul[1,2*], Jorge Miguel Sampaio[3,4], Salim Daoudi[1,2], José Pires Marques[3,4], Fernando Parente[5], Assala Hamidani[1,2], Stephen Croft[6], Andrea Favalli[7,8], Yazid Kasri[9], Amina Zidi[1,2], Kahina Amari[1,2]

[1]*Department of Matter Sciences, Faculty of Sciences and Technology, Mohamed El Bachir El Ibrahimi University, Bordj-Bou-Arreridj 34030, Algeria.*
[2]*Laboratory of Materials Physics, Radiation and Nanostructures (LPMRN), Faculty of Sciences and Technology, Mohamed El Bachir El Ibrahimi University, Bordj-Bou-Arreridj 34030, Algeria.*
[3]*LIP – Laboratório de Instrumentação e Física Experimental de Partículas, Av. Prof. Gama Pinto 2, 1649-003 Lisboa, Portugal.*
[4]*Faculdade de Ciências da Universidade de Lisboa, Campo Grande, C8, 1749-016 Lisboa, Portugal.*
[5]*Laboratory of Instrumentation, Biomedical Engineering and Radiation Physics (LIBPhys-UNL), Department of Physics, NOVA School of Science and Technology, NOVA University Lisbon, 2829-516 Caparica, Portugal.*
[6]*School of Engineering, Faculty of Science of Technology, Nuclear Science & Engineering Research Group, Lancaster University, Bailrigg, Lancaster, LA1 4YW, United Kingdom.*
[7]*European Commission, Joint Research Centre, Ispra, I-21027, Italy.*
[8]*Los Alamos National Laboratory, P.O. Box 1663, Los Alamos, NM 87545, USA.*
[9]*Theoretical Physics Laboratory, University of Bejaia, 06000 Bejaia, Algeria.*
[*]Corresponding author. Tel. /Fax (+213) 035862230.
E-mail address: a.kahoul@univ-bba.dz; ahalim.kahoul@gmail.com

Abstract:

In this study, we use the relativistic multiconfiguration Dirac–Fock method (MCFD) to compute the probabilities of radiative and radiationless vacancy transfer from K- to L_1-, L_2-, and L_3- subshells in $_{16}$S, $_{18}$Ar, $_{22}$Ti, $_{29}$Cu, $_{30}$Zn, $_{32}$Ge, $_{33}$As, $_{34}$Se, $_{36}$Kr, $_{40}$Zr, $_{48}$Cd, $_{50}$Sn, $_{52}$Te, $_{80}$Hg, $_{83}$Bi, and $_{86}$Rn atoms. Semi-theoretical calculations for elements within the atomic range of $18 \leq Z \leq 96$ ($_{18}$Ar to $_{96}$Cm) were also conducted, leveraging available data on radiative and radiationless transitions from the scientific literature. The theoretical calculation results aligned well with the values calculated semi-theoretically and with other published works. However, some notable differences were identified.

Keywords: Relativistic calculation, MCDF method, vacancy transfer probabilities, K-shell transitions.

1. Introduction

An ionized atom, in our case with a K-shell vacancy, is an inherently unstable electronic configuration. Subsequently, this instability can result in either a radiative transition or an Auger process, which is a radiationless transition. In both decay modes, the initial vacancy in the inner shell is transferred to a higher shell or subshell, potentially giving rise to additional vacancies in higher shells. This cascade of vacancies persists until all vacancies reach the outermost occupied shell [1]. The K- to L-shell/subshell vacancy transfer probabilities denote the mean number of vacancies generated in the L-shell/subshell for each vacancy in the K-shell. Understanding these parameters holds crucial significance across various scientific disciplines, including physics, chemistry, medical research, and nuclear science and technology. Their applications span a wide spectrum, including X-ray spectroscopy, plasma physics, astrophysics, materials science, radiation dosimetry, plasma characterization, radiation protection, and industrial radiation processing. Numerous computations have been conducted to estimate both radiative and radiationless vacancy transfer probabilities. Rao et al. [2] specifically focused on calculating the average number of primary L_n subshell vacancies resulting from electron transitions to the K-shell for elements with atomic numbers range of $20 \leq Z \leq 96$, and Bambynek et al. [3] reviewed the situation. Puri et al. [1] performed calculations for the total K-shell to L_1-, L_2-, and L_3-subshell vacancy transfer probabilities (η_{KL_n}), encompassing elements with atomic numbers $18 \leq Z \leq 96$, using the theoretical radiative transition rates of Scofield [4] and radiationless transition rates tabulated by Chen et al. [5]. Schönfeld and Janßen [6] compiled a table of semi-empirical data for K- to L-shell ($\eta_{\mathrm{KL}}^{\mathrm{T}}$) total vacancy transfer probabilities, covering elements with atomic numbers $10 \leq Z \leq 100$. Sampaio et al. [7] utilized the Dirac–Fock method to compute the total K-shell to L_1-, L_2-, and L_3-subshell vacancy transfer probabilities (η_{KL_n}) for Zn, Cd, and Hg. Berkani et al. [8] interpolated the experimental data using an analytical

function to deduce the empirical values for the atomic parameters η_{KM}^{T}, $\eta_{KL_2}^{R}$, $\eta_{KL_3}^{R}$, and η_{KM}^{R} of vacancy transfer probabilities in the atomic range of $16 \leq Z \leq 92$.

While numerous studies have provided K- to L-shell/subshell vacancy transition probabilities with commendable accuracy across various elements, particularly in the low to medium atomic number (Z) range, notable gaps persist for heavier elements where relativistic and electron correlation effects are more pronounced. Current models and data often overlook the complex interactions in these higher-Z regions, leading to potential inaccuracies in predictions involving radiationless transitions and electron rearrangements. More recently, more sophisticated methods and computer codes were developed to calculate atomic parameters such as energies and transition probabilities.

In this study, we present calculated results for radiative vacancy transfer probabilities ($\eta_{KL_2}^{R}$, $\eta_{KL_3}^{R}$, and η_{KL}^{R}), using a state-of-art computer code, including quantum electron dynamic (QED) contributions. Noteworthy, the values of $\eta_{KL_1}^{R}$ have been omitted from consideration due to their negligible contribution. This is because the electric-dipole selection rule forbids the radiative K-L1 transitions, $\Delta l = \pm 1$, wherein (Δl) denotes the change in the hole orbital angular momentum. The strict adherence to this selection rule significantly diminishes the likelihood of such transitions, making their impact on the overall quantities $\eta_{KL_1}^{R}$ inconsequential. Additionally, the study encompasses radiationless (Auger) ($\eta_{KL_1}^{A}$, $\eta_{KL_2}^{A}$, $\eta_{KL_3}^{A}$, and η_{KL}^{A}), and η_{KL}^{T} total vacancy transfer probabilities. Initially, relativistic calculations were conducted using the multiconfiguration Dirac–Fock method (MCFD) computer code MCDFGME, as developed by Desclaux and Indelicato [9–11]. This approach was applied to $_{16}$S, $_{18}$Ar, $_{22}$Ti, $_{29}$Cu, $_{30}$Zn, $_{32}$Ge, $_{33}$As, $_{34}$Se, $_{36}$Kr, $_{40}$Zr, $_{48}$Cd, $_{50}$Sn, $_{52}$Te, $_{80}$Hg, $_{83}$Bi, and $_{86}$Rn atoms. Subsequently, for comparative purposes, semi-theoretical calculations were performed for elements within the atomic number range of $18 \leq Z \leq 96$. These calculations were based on radiative transition rates

extracted from Scofield [4] and radiationless transition rates fitted using the Auger transition rates reported by Chen et al. [5].

2. Basic Relationships

The vacancy-transfer probabilities, denoted as η_{KL_n} ($n = 1,2,3$), are defined as the average number of primary L_i-subshell vacancies produced in the decay of a K-shell vacancy through radiative and radiationless (Auger) transitions of the types K-L$_n$*X* (*X*= L, M, N, O, ...). This definition specifically excludes the L_i subshell vacancies produced through a Coster-Kronig transition of the type L$_n$-L$_m$*X* ($X \neq$ L). It is noteworthy that Coster-Kronig (CK) transitions do not change the total K- to L-shell vacancy transfer probability. The values of η_{KL_n} have been computed using the equations provided by Rao et al. [2]:

$$\eta^{\mathrm{T}}_{\mathrm{KL}_n} = \frac{\Gamma^{\mathrm{R}}_{\mathrm{KL}_n}}{\Gamma^{\mathrm{R}}_{\mathrm{K}}+\Gamma^{\mathrm{A}}_{\mathrm{K}}} + \frac{2\Gamma^{\mathrm{A}}_{\mathrm{K,L}_n\mathrm{L}_n}+\sum_{m(X_m\neq \mathrm{L}_n)}\Gamma^{\mathrm{A}}_{\mathrm{K,L}_nX_m}}{\Gamma^{\mathrm{R}}_{\mathrm{K}}+\Gamma^{\mathrm{A}}_{\mathrm{K}}} = \eta^{\mathrm{R}}_{\mathrm{KL}_n} + \eta^{\mathrm{A}}_{\mathrm{KL}_n}, \quad (1)$$

and

$$\eta^{\mathrm{R}}_{\mathrm{KL}} = \sum_{n=1}^{3}\eta^{\mathrm{R}}_{\mathrm{KL}_n} \quad (2)$$

$$\eta^{\mathrm{A}}_{\mathrm{KL}} = \sum_{n=1}^{3}\eta^{\mathrm{A}}_{\mathrm{KL}_n} \quad (3)$$

$$\eta^{\mathrm{T}}_{\mathrm{KL}} = \sum_{n=1}^{3}\eta^{\mathrm{T}}_{\mathrm{KL}_n} = \eta^{\mathrm{R}}_{\mathrm{KL}} + \eta^{\mathrm{A}}_{\mathrm{KL}}. \quad (4)$$

Here, $\Gamma^{\mathrm{R}}_{\mathrm{KL}_n}$ represents the partial width associated with the radiative transition from the K-shell vacancy to the L$_n$ subshell, and $\Gamma^{\mathrm{A}}_{\mathrm{K,L}_nX_m}$ represents the partial width corresponding to the radiationless (Auger) transition from the K-shell vacancy to a L$_n$ subshell and the creation of another vacancy in an *X* subshell (where $m \neq n$ if *X* = L). $\Gamma^{\mathrm{R}}_{\mathrm{K}}$ and $\Gamma^{\mathrm{A}}_{\mathrm{K}}$ are, respectively, the radiative and radiationless (Auger) K- shell widths, and $\Gamma_{\mathrm{K}} = \Gamma^{\mathrm{R}}_{\mathrm{K}} + \Gamma^{\mathrm{A}}_{\mathrm{K}}$, is the corresponding total width. The statistical weight 2 in the term $\Gamma^{\mathrm{A}}_{\mathrm{K,L}_n\mathrm{L}_n}$ takes into account the possibility that radiationless transitions can create two vacancies in the same subshell L$_n$. η_{KL_n} represents the

probability of total vacancy transfer between the K shell and the L_n subshell, where T, R , and A stand, respectively, for the total, radiative and radiationless (Auger) probabilities.

3. Relativistic calculations

3.1 Multiconfiguration Dirac–Fock method (MCDF)

The MCDF (Multiconfiguration Dirac-Fock) is a method for obtaining energy level energies and transition probabilities within a relativistic atomic system. This method is implemented through the MCDFGME code, developed by Desclaux and Indelicato [9–11].

The relativistic Dirac-Coulomb-Breit Hamiltonian (H_{DCB}) describing the *N*-electron system is expressed in the form:

$$H_{\mathrm{DCB}} = \sum_{i=1}^{N} h_i^{\mathrm{D}} + \sum_{i=1}^{N-1} \sum_{j=i+1}^{N} V_{ij}^{\mathrm{CB}}. \quad (5)$$

Here, the first term on the right side represents the sum of *N* one-electron Dirac Hamiltonian operators h_i^{D}; the second term is the combined Coulomb repulsion and Breit interaction (V_{ij}^{CB}) between distinct pairs of electrons (*i*,*j*) where $j > i$. The atomic wave function $|\Psi_{\Pi,\mathrm{J},\mathrm{M}}\rangle$ is obtained by solving the following equation in the presence of the relativistic Hamiltonian H_{DCB}

$$H_{\mathrm{DCB}}|\Psi_{\Pi,J,M}\rangle = \mathrm{E}_{\Pi,J,M}|\Psi_{\Pi,J,M}\rangle, \quad (6)$$

where $\mathrm{E}_{\Pi,J,M}$ represents the corresponding energy eigenvalue. The symbols Π, J, M represent quantum numbers that characterize the state of the atomic system:

- Π represents the parity of the state,
- J represents the total angular momentum quantum number,
- M represents the magnetic quantum number associated with the *z*-axis component of the angular momentum

The wavefunction can be expressed as a linear combination of configuration state functions (CSFs) [12].

$$\left|\Psi_{\Pi,J,M}\right\rangle = \sum_n C_n(\Pi, J, M) \left|\Phi_{\Pi,J,M}(\gamma_n)\right\rangle. \quad (7)$$

Here, C_n are the configuration mixing coefficients for the atomic state, and γ_n represent all information necessary to uniquely define the CSFs. These equations illustrate the foundational principles of the MCDF method, where the atomic wave function is represented as a superposition of different configurations, each associated with a specific energy and contributing to the overall quantum state. Solving the equation with the relativistic Hamiltonian allows for the determination of both the energy levels and the corresponding wave functions. Further details can be found in [13–16].

In our calculations, however, a single electronic configuration approach was employed, meaning that only one CSF is included in the summation. It is important to note, however, that the CSF results, in turn, from the linear combination of several Slater determinants of one-electron Dirac spinors, with the same Π and J.

We must note that the computational cost (as well as convergence issues) increases rapidly with the number of CSFs included, making calculations of many-electron systems beyond single configuration very time-consuming. Also, as the approximation used for the evaluation of the radiationless transition probabilities cannot be used in the so-called optimized level (OL) scheme with full multiconfiguration wave functions, our correlated atomic state functions do not go beyond the approximation referred to above. This simplification should have little effect on internal transitions in many-electron and closed-shell systems, since, in these cases, the ground-state CSF dominates.

The Breit interaction and vacuum polarization terms were accounted for in the self-consistent field process, while other quantum electrodynamics (QED) effects were included as

perturbations. For a more in-depth understanding of the QED corrections used, we direct the reader to the reference by Mohr et al. [17]. Nuclear core size effects are taken in account by employing a uniformly distributed charge sphere [18].

Radiative transition probabilities are obtained using the formalism proposed by Löwdin et al. [19] to treat the non-orthogonality effects of the initial and final state wave functions obtained independently in the OL method. The length gauge is adopted for all radiative transition calculations.

In what concerns the radiationless (Auger and Coster-Kronig) transitions, it is assumed that the inner-shell hole creation is independent of the decay process. The final state continuum-electron wave functions are derived by solving the Dirac-Fock equations using the same atomic potential as for the initial state. In this calculation, no orbital relaxation is permitted between the initial and final bound state wave functions, meaning that the equations or methods used do not take into account changes in the shapes of electronic orbitals during the transition. In simpler terms, the calculations assume that spectator electrons remain in their original orbitals without undergoing significant change during the transition. This approximation, while not exact, allows for maintaining the orthogonality between initial and final wave functions and significantly simplifies calculations.

3.2 Linewidths and vacancy transfer probabilities

To calculate vacancy transfer probabilities, we compute the width Γ_i of an atomic level *i*, defined by a Π_i and J_i values for a given one-hole configuration, summing the allowed transition probabilities from this level to all lower-energy levels. This summation encompasses both radiative transitions (W^{R}_{i,j_1}, involving the emission of a photon) and radiationless transitions (W^{A}_{i,j_2}, involving the emission of an electron), multiplied by the reduced Planck constant $\hbar$ [20–22].

$$\Gamma_{\mathrm{K}} = \hbar\left(\sum_{j_1} W^{\mathrm{R}}_{i,j_1} + \sum_{j_2} W^{\mathrm{A}}_{i,j_2}\right) = \sum_{j_1} \Gamma^{\mathrm{R}}_{i,j_1} + \sum_{j_2} \Gamma^{\mathrm{A}}_{i,j_2}. \quad (8)$$

This equation quantifies the overall broadening or width of the atomic level *i*. The summations are performed over all possible final states, where the index j_1 represents all one-hole levels that the initial level *i* can decay to radiatively, and the index j_2 represents all two-hole levels that the level *i* can decay to via radiationless (Auger) emission. If the system has no unpaired outer electrons, or if the interaction between the hole and those electrons is neglected, only one level corresponds to each one-hole configuration. Therefore, the width of the configuration is just the width of the corresponding level. This scenario simplifies the analysis, as the absence of interactions results in a direct correlation between the width of the configuration and the width of the individual level, where width and lifetime are inversely related.

The situation becomes more intricate when the interaction with existing unpaired electrons is considered. The fine structure resulting from the interaction between the inner hole and these electrons leads to several different levels for a given configuration [23]. In such cases, the width of the configuration is influenced by the intricate interplay between the inner hole and the surrounding unpaired electrons, giving rise to a richer and more nuanced spectrum of levels within the configuration. This complexity underscores the importance of considering electron interactions when analyzing the width of atomic configurations [20,21].

Assuming that the initial levels in the K shell with total angular momentum J_i, are statistically populated, its radiative width $\Gamma^{\mathrm{R}}_{\mathrm{K}}$ is obtained by summing the partial widths $\Gamma^{\mathrm{R}}_{i,j_1}$ for all levels *i* of the system with one hole in this shell decaying radiatively to all levels j_1 of the system with one hole in a higher subshell [21,23].

$$\Gamma^{\mathrm{R}}_{\mathrm{K}} = \frac{\sum_i \sum_{j_1} (2J_i+1)\Gamma^{\mathrm{R}}_{i,j_1}}{\sum_i (2J_i+1)}. \quad (9)$$

In the same way, the radiationless width of the K shell is given by

$$\Gamma_{\mathrm{K}}^{\mathrm{A}} = \frac{\sum_i \sum_{j_2} (2J_i+1)\Gamma_{i,j_2}^{\mathrm{A}}}{\sum_i (2J_i+1)}\,. \tag{10}$$

Here, $\Gamma_{i,j_2}^{\mathrm{A}}$ is the partial width corresponding to the Auger transition from level *i* in the system with one hole in K shell to level j_2 in the system with two holes in higher shells or subshells, with the emission of an electron to the continuum. The total width of the K-shell is given by

$$\Gamma_{\mathrm{K}} = \Gamma_{\mathrm{K}}^{\mathrm{R}} + \Gamma_{\mathrm{K}}^{\mathrm{A}}. \tag{11}$$

The vacancy transfer probabilities specified in Section 2 by equation (1) can be redefined in this case and presented in the following manner:

$$\eta_{\mathrm{KL}_n}^{\mathrm{T}} = \frac{\sum_i \sum_{j_1} (2J_i+1)\Gamma_{i,j}^{\mathrm{R}}}{\sum_i (2J_i+1)\left[\sum_{j_1} \Gamma_{i,j_1}^{\mathrm{R}} + \sum_{j_2} \Gamma_{i,j_2}^{\mathrm{A}}\right]} + \frac{\sum_i (2J_i+1)\left[2\sum_{j'} \Gamma_{i,j'}^{\mathrm{A}} + \sum_{j''} \Gamma_{i,j''}^{\mathrm{A}}\right]}{\sum_i (2J_i+1)\left[\sum_{j_1} \Gamma_{i,j_1}^{\mathrm{R}} + \sum_{j_2} \Gamma_{i,j_2}^{\mathrm{A}}\right]}$$

$$= \frac{\sum_i \sum_{j_1} (2J_i+1)\Gamma_{i,j}^{\mathrm{R}}}{\Gamma_{\mathrm{K}}^{\mathrm{R}} + \Gamma_{\mathrm{K}}^{\mathrm{A}}} + \frac{\sum_i (2J_i+1)\left[2\sum_{j'} \Gamma_{i,j'}^{\mathrm{A}} + \sum_{j''} \Gamma_{i,j''}^{\mathrm{A}}\right]}{\Gamma_{\mathrm{K}}^{\mathrm{R}} + \Gamma_{\mathrm{K}}^{\mathrm{A}}}$$

$$= \eta_{\mathrm{KL}_n}^{\mathrm{R}} + \eta_{\mathrm{KL}_n}^{\mathrm{A}}, \tag{12}$$

where *i* is the initial one-hole level in the K-shell and *j* is a final one-hole level in the L_n subshell (n=1,2,3), whereas j' are two-hole in the $\mathrm{L}_n\mathrm{L}_n$ and j'' are two-hole levels in the $\mathrm{L}_n\mathrm{L}_m$ ($n \neq m$ if X=L) subshells, respectively.

The present relativistic calculations of radiative $\eta_{\mathrm{KL}_2}^{\mathrm{R}}$, $\eta_{\mathrm{KL}_3}^{\mathrm{R}}$, and $\eta_{\mathrm{KL}}^{\mathrm{R}}$ and additionally, the radiationless $\eta_{\mathrm{KL}_1}^{\mathrm{A}}$, $\eta_{\mathrm{KL}_2}^{\mathrm{A}}$, $\eta_{\mathrm{KL}_3}^{\mathrm{A}}$, and $\eta_{\mathrm{KL}}^{\mathrm{A}}$, and $\eta_{\mathrm{KL}}^{\mathrm{T}}$ total vacancy transfer probabilities using the equations (12, 2,3 and 4) for the previously mentioned elements are listed in Table 1.

4. Semi-theoretical calculations

In this study, semi-theoretical calculations were undertaken to determine the values of radiative $\eta_{\mathrm{KL}_2}^{\mathrm{R}}$, $\eta_{\mathrm{KL}_3}^{\mathrm{R}}$, and $\eta_{\mathrm{KL}}^{\mathrm{R}}$, and additionally, the radiationless $\eta_{\mathrm{KL}_1}^{\mathrm{A}}$, $\eta_{\mathrm{KL}_2}^{\mathrm{A}}$, $\eta_{\mathrm{KL}_3}^{\mathrm{A}}$, and $\eta_{\mathrm{KL}}^{\mathrm{A}}$, and $\eta_{\mathrm{KL}}^{\mathrm{T}}$ total vacancy transfer probabilities for elements in the atomic range of $18 \leq Z \leq 96$. These

calculations were executed using equations (1, 2, 3, and 4) and are presented in Table 3. The K-shell radiative rates were obtained directly from Scofield [4] tabulated values, based on the relativistic Hartree-Slater theory, and used as a reference for calculating radiative vacancy transfer probabilities across the atomic range covered in this study. Subsequently, the radiationless transition widths (Auger), based on the relativistic Dirac-Hartree-Slater model reported by Chen et al. [5], were fitted (all points equally weighted in a least square algorithm) using the analytical function

$$(\Gamma_{\mathrm{K}-XY})_{\mathrm{S-theo}} = \hbar\,(\mathrm{W}_{\mathrm{K}-XY})_{\mathrm{S-theo}} = \hbar(\sum_{r=0}^{5} A_r\, Z^r), \tag{13}$$

where XY represents the final two-hole state, $\mathrm{W}_{\mathrm{K}-XY}$ represents the radiationless transition probabilities from K-shell to the final two-hole state XY. The fitting coefficients A_r for all possible final two-hole states are listed in Table 2, with coefficients expressed in milliatomic units (ma.u), where $1\mathrm{ma.u} = 0.02721\ \frac{\mathrm{eV}}{\hbar} = 4.134 \times 10^{13} s^{-1}$.

It is essential to emphasize that the fitting equation (13) and its associated coefficients are valid only within the region covered by the utilized theoretical data [5]. Extending these fittings beyond the specified ranges may result in erroneous estimates for the radiationless (Auger) transition width.

The semi-theoretical approach complements the Dirac-Fock calculations by providing vacancy transfer probabilities over a wide atomic range ($18 \leq Z \leq 96$), balancing computational feasibility and accuracy. While recent work [8] has presented empirical vacancy transfer probabilities derived from experimental data, this semi-theoretical method bridges gaps where experimental data are sparse or limited to specific atomic regions. It thus serves as a comparative benchmark to verify the accuracy of fully theoretical predictions for both radiative and Auger transitions.

Using Scofield [4] radiative data and Chen et al. [5] Auger data as the basis, we generated a continuous function of Z via polynomial fitting. This fitting process smooths out minor inconsistencies that may arise from discrete tabulated data, enhancing the robustness of transition probability estimates across the atomic range. The polynomial function also reduces the impact of localized uncertainties and provides an analytical form for transition probabilities, enabling straightforward calculations for any atomic number within the range of interest. Additionally, it allows us to estimate values for atomic numbers not explicitly calculated by Scofield [4] and Chen et al. [5] or where data are otherwise unavailable.

5. Results and discussion

Theoretical and semi-theoretical values for the parameters ($\eta^{\mathrm{R}}_{\mathrm{KL}_2}$, $\eta^{\mathrm{R}}_{\mathrm{KL}_3}$, $\eta^{\mathrm{R}}_{\mathrm{KL}}$, $\eta^{\mathrm{A}}_{\mathrm{KL}_1}$, $\eta^{\mathrm{A}}_{\mathrm{KL}_2}$, $\eta^{\mathrm{A}}_{\mathrm{KL}_3}$, $\eta^{\mathrm{A}}_{\mathrm{KL}}$, and $\eta^{\mathrm{T}}_{\mathrm{KL}}$ are listed in Tables 1 and 3, respectively. The radiationless vacancy transfer probabilities, denoted as $\eta^{\mathrm{A}}_{\mathrm{KL}_1}$, $\eta^{\mathrm{A}}_{\mathrm{KL}_2}$, $\eta^{\mathrm{A}}_{\mathrm{KL}_3}$, and $\eta^{\mathrm{A}}_{\mathrm{KL}}$, were assessed for elements with atomic numbers in the range $18 \leq Z \leq 96$. The obtained values, both relativistic and semi-theoretical, are plotted in Fig. 1 according to the atomic number Z along with the values tabulated by Rao et al. [2]. Panels (a), (b), (c), and (d) represent $\eta^{\mathrm{A}}_{\mathrm{KL}_1}$, $\eta^{\mathrm{A}}_{\mathrm{KL}_2}$, $\eta^{\mathrm{A}}_{\mathrm{KL}_3}$, and $\eta^{\mathrm{A}}_{\mathrm{KL}}$ respectively. The comparison illustrates a general agreement between the theoretical and semi-theoretical results. However, some notable deviations are observed. The theoretical values exhibit a maximum deviation of 9% for $_{18}$Ar, 30% for $_{30}$Zn, 37% for $_{29}$Cu and $_{30}$Zn, and 15% for $_{86}$Rn across the parameters $\eta^{\mathrm{A}}_{\mathrm{KL}_1}$, $\eta^{\mathrm{A}}_{\mathrm{KL}_2}$, $\eta^{\mathrm{A}}_{\mathrm{KL}_3}$, and $\eta^{\mathrm{A}}_{\mathrm{KL}}$, respectively. Furthermore, a comparison with the values from Rao et al. [2] reveals good overall agreement, with a notable exception. A significant deviation is observed in the parameter $\eta^{\mathrm{A}}_{\mathrm{KL}_2}$, amounting to 79%, 70%, and 63% for elements $_{20}$Ca, $_{22}$Ti, and $_{24}$Cr, respectively. Similarly, a 31% deviation is noted for $_{22}$Ti compared to our theoretical results. In the case of $\eta^{\mathrm{A}}_{\mathrm{KL}_3}$, a 38% deviation is observed for $_{20}$Ca concerning the semi-theoretical results. The observed deviation between semi-theoretical and Rao et al. [2]

values in certain elements are attributed to the increasing competition between electrostatic and spin-orbit interactions. The limitations of the Dirac-Hartree-Slater (DHS) model become apparent in this atomic region, as it proves insufficient to fully explain the Auger transfer rates. The total radiationless vacancy transfer probability η_{KL}^{A} demonstrates strong alignment among theoretical, semi-theoretical, and Rao et al. [2] values, as illustrated in Fig. 1(d). Regarding the comparison of our semi-theoretical results with the experimental values reported by Ertuğrul [24,25] and Han et al. [26], we observe a good level of agreement overall. However, deviations are noted for certain elements: 15% for $_{56}$Ba and 14% for $_{63}$Eu with respect to $\eta_{KL_1}^{A}$, 11% for $_{57}$La for $\eta_{KL_2}^{A}$, 22% for $_{56}$Ba and 13% for $_{59}$Pr for $\eta_{KL_3}^{A}$, and 12% for $_{56}$Ba for η_{KL}^{A}, and it is important to note that we found no experimental values available for the range of atomic elements on which we calculated the theoretical probabilities of radiationless vacancy transfer from the K- to L-shell.

Fig. 2 presents the theoretical, semi-theoretical, Rao et al. [2], and empirical values from Berkani et al. [8] values of radiative vacancy transfer probabilities with respect to the atomic number *Z*. Panels (a), (b), and (c) represent $\eta_{KL_2}^{R}$, $\eta_{KL_3}^{R}$, and η_{KL}^{R} respectively, while panel (d) present η_{KL}^{T}. The panels for the radiative probability parameters demonstrated closer agreement compared to the Auger parameters, with deviations not exceeding 2% when comparing the theoretical values with those of Rao et al. [2], 5% when comparing the semi-theoretical values with Rao et al. [2], and 4% and 5% when comparing the theoretical and semi-theoretical values with the empirical values of Berkani et al. [8], respectively. Additionally, a 6% deviation was observed when comparing the theoretical values with the semi-theoretical ones. The total vacancy transfer probabilities η_{KL}^{T} also exhibited remarkable agreement, with deviations not exceeding 6% when comparing the values with each other. Moreover, it is noteworthy that the radiationless vacancy transfer probabilities exhibit a decreasing trend with increasing atomic number *Z*, while conversely, the radiative transition probabilities show a rising trend with *Z*.

This observation adds valuable insights into the behavior of these probabilities in relation to the atomic structure, particularly for high-Z elements. Our findings indicate that radiative transition probabilities increase with Z, while non-radiative (Auger) probabilities decrease. This trend reflects the impact of a stronger Coulomb field in high-Z atoms, which favors photon over electron emission. Relativistic effects, including spin-orbit coupling, further shape these transitions by splitting L-subshell energy levels, particularly enhancing radiative transitions in heavier elements. The Multi-Configuration Dirac-Fock (MCDF) method captures these relativistic interactions and electron correlations, allowing a realistic calculation of vacancy transfer probabilities. This approach provides predictive insights valuable for interpreting X-ray and Auger spectra in atomic physics and applications like nuclear medicine. Overall, the results confirm theoretical trends, while highlighting the balance between radiative and Auger yields across a broad atomic range.

6. Conclusion

The relativistic calculations conducted for elements $_{16}$S, $_{18}$Ar, $_{22}$Ti, $_{29}$Cu, $_{30}$Zn, $_{32}$Ge, $_{33}$As, $_{34}$Se, $_{36}$Kr, $_{40}$Zr, $_{48}$Cd, $_{50}$Sn, $_{52}$Te, $_{80}$Hg, $_{83}$Bi, and $_{86}$Rn using the multiconfiguration Dirac-Fock code developed by Desclaux and Indelicato, along with the semi-theoretical calculations for elements within the atomic range of $18 \leq Z \leq 96$ utilizing radiative data proposed by Scofield [4] and radiationless data introduced by Chen et al. [5] for vacancy transfer probabilities from K-shell to L-shell/subshell, exhibit a commendable level of agreement among themselves and align well with the established values of Rao et al. [2]. However, the radiationless calculations show some deviations, particularly in the semi-theoretical approach. This can be attributed to the fact that the Dirac-Hartree-Slater (DHS) models are based the mean-field approach whereas the multiconfiguration Dirac-Fock (MCDF) method, even in the single-configuration approach used in this work, considers some degree of electronic correlation. This is especially important for low atomic number elements with unpaired electrons where the largest deviations are

observed. We propose that theoretical and semi-theoretical investigations into these fundamental parameters should be extended to include additional elements and shells, in order to further our understanding of atomic inner-shell ionization processes.

Figures caption:

Fig. 1. Comparison of current theoretical and semi-theoretical vacancy transfer probabilities $\eta^{\mathrm{A}}_{\mathrm{KL}_1}$, $\eta^{\mathrm{A}}_{\mathrm{KL}_2}$, $\eta^{\mathrm{A}}_{\mathrm{KL}_3}$, and $\eta^{\mathrm{A}}_{\mathrm{KL}}$ as a function of atomic number *Z*, with those of Rao et al. [2].

Fig. 2. Comparison of current theoretical and semi-theoretical vacancy transfer probabilities $\eta^{\mathrm{R}}_{\mathrm{KL}_2}$, $\eta^{\mathrm{R}}_{\mathrm{KL}_3}$, $\eta^{\mathrm{R}}_{\mathrm{KL}}$, and $\eta^{\mathrm{T}}_{\mathrm{KL}}$ as a function of atomic number *Z*, with those of Rao et al. [2] and Berkani et al. [8].

References:

[1] S. Puri, D. Mehta, B. Chand, N. Singh, J.H. Hubbell, P.N. Trehan, Production of L, subshell and M shell vacancies following inner-shell vacancy production, Nuclear Instruments and Methods in Physics Research B 83 (1993) 21–30. https://doi.org/10.1016/0168-583X(93)95902-H.

[2] P.V. Rao, M.H. Chen, B. Crasemann, Atomic Vacancy Distributions Produced by Inner-Shell Ionization, Phys. Rev. A 5 (1972) 997–1012. https://doi.org/10.1103/PhysRevA.5.997.

[3] W. Bambynek, B. Crasemann, R.W. Fink, H.-U. Freund, H. Mark, C.D. Swift, R.E. Price, P.V. Rao, X-Ray Fluorescence Yields, Auger, and Coster-Kronig Transition Probabilities, Rev. Mod. Phys. 44 (1972) 716–813. https://doi.org/10.1103/RevModPhys.44.716.
[4] J.H. Scofield, Relativistic hartree-slater values for K and L X-ray emission rates, Atomic Data and Nuclear Data Tables 14 (1974) 121–137. https://doi.org/10.1016/S0092-640X(74)80019-7.
[5] M.H. Chen, B. Crasemann, H. Mark, Relativistic radiationless transition probabilities for atomic K- and L-shells, Atomic Data and Nuclear Data Tables 24 (1979) 13–37. https://doi.org/10.1016/0092-640X(79)90037-8.
[6] E. Schönfeld, H. JanBen, Evaluation of atomic shell data, Nuclear Instruments and Methodsin PhysicsResearchA 369 (1996) 527–533.
[7] J.M. Sampaio, M. Guerra, F. Parente, T.I. Madeira, P. Indelicato, J.P. Santos, J.P. Marques, Calculations of photo-induced X-ray production cross-sections in the energy range 1–150 keV and average fluorescence yields for Zn, Cd and Hg, Atomic Data and Nuclear Data Tables 111–112 (2016) 67–86. https://doi.org/10.1016/j.adt.2016.02.001.
[8] B. Berkani, A. Kahoul, J.M. Sampaio, S. Daoudi, J.P. Marques, F. Parente, A. Hamidani, S. Croft, A. Favalli, Y. Kasri, A. Zidi, K. Amari, Vacancy transfer probability parameters: Database and a new empirical value for elements in the atomic number range $16 \leq Z \leq 92$, Radiation Physics and Chemistry 225 (2024) 112106. https://doi.org/10.1016/j.radphyschem.2024.112106.
[9] J.P. Desclaux, A multiconfiguration relativistic DIRAC-FOCK program, Computer Physics Communications 9 (1975) 31–45. https://doi.org/10.1016/0010-4655(75)90054-5.
[10] O. Gorceix, P. Indelicato, J.P. Desclaux, Multiconfiguration Dirac-Fock studies of two-electron ions. I. Electron-electron interaction, J. Phys. B: At. Mol. Phys. 20 (1987) 639–649. https://doi.org/10.1088/0022-3700/20/4/006.
[11] P. Indelicato, J.P. Desclaux, Multiconfiguration Dirac-Fock calculations of transition energies with QED corrections in three-electron ions, Phys. Rev. A 42 (1990) 5139–5149. https://doi.org/10.1103/PhysRevA.42.5139.
[12] I.P. Grant, Relativistic atomic structure theory: Some recent work, Int J of Quantum Chemistry 25 (1984) 23–46. https://doi.org/10.1002/qua.560250104.
[13] I.P. Grant, H.M. Quiney, Foundations of the Relativistic Theory of Atomic and Molecular Structure, in: Advances in Atomic and Molecular Physics, Elsevier, 1988: pp. 37–86. https://doi.org/10.1016/S0065-2199(08)60105-0.
[14] K.G. Dyall, I.P. Grant, C.T. Johnson, F.A. Parpia, E.P. Plummer, GRASP: A general-purpose relativistic atomic structure program, Computer Physics Communications 55 (1989) 425–456. https://doi.org/10.1016/0010-4655(89)90136-7.
[15] P. Indelicato, Projection operators in multiconfiguration Dirac-Fock calculations: Application to the ground state of heliumlike ions, Phys. Rev. A 51 (1995) 1132–1145. https://doi.org/10.1103/PhysRevA.51.1132.
[16] F.A. Parpia, C.F. Fischer, I.P. Grant, GRASP92: A package for large-scale relativistic atomic structure calculations, Computer Physics Communications 94 (1996) 249–271. https://doi.org/10.1016/0010-4655(95)00136-0.
[17] P.J. Mohr, G. Plunien, G. Soff, QED corrections in heavy atoms, Physics Reports 293 (1998) 227–369. https://doi.org/10.1016/S0370-1573(97)00046-X.
[18] I. Angeli, K.P. Marinova, Table of experimental nuclear ground state charge radii: An update, Atomic Data and Nuclear Data Tables 99 (2013) 69–95. https://doi.org/10.1016/j.adt.2011.12.006.

[19] P.-O. Löwdin, Quantum Theory of Many-Particle Systems. I. Physical Interpretations by Means of Density Matrices, Natural Spin-Orbitals, and Convergence Problems in the Method of Configurational Interaction, Phys. Rev. 97 (1955) 1474–1489. https://doi.org/10.1103/PhysRev.97.1474.
[20] K. Kozioł, MCDF-RCI predictions for structure and width of K α 1 , 2 x-ray line of Al and Si, Journal of Quantitative Spectroscopy and Radiative Transfer 149 (2014) 138–145. https://doi.org/10.1016/j.jqsrt.2014.08.009.
[21] M. Guerra, J.M. Sampaio, T.I. Madeira, F. Parente, P. Indelicato, J.P. Marques, J.P. Santos, J. Hoszowska, J.-Cl. Dousse, L. Loperetti, F. Zeeshan, M. Müller, R. Unterumsberger, B. Beckhoff, Theoretical and experimental determination of L -shell decay rates, line widths, and fluorescence yields in Ge, Phys. Rev. A 92 (2015) 022507. https://doi.org/10.1103/PhysRevA.92.022507.
[22] M. Guerra, J.M. Sampaio, G.R. Vília, C.A. Godinho, D. Pinheiro, P. Amaro, J.P. Marques, J. Machado, P. Indelicato, F. Parente, J.P. Santos, Fundamental Parameters Related to Selenium Kα and Kβ Emission X-ray Spectra, Atoms 9 (2021) 8. https://doi.org/10.3390/atoms9010008.
[23] M. Guerra, J.M. Sampaio, F. Parente, P. Indelicato, P. Hönicke, M. Müller, B. Beckhoff, J.P. Marques, J.P. Santos, Theoretical and experimental determination of K - and L - shell x-ray relaxation parameters in Ni, Phys. Rev. A 97 (2018) 042501. https://doi.org/10.1103/PhysRevA.97.042501.
[24] M. Ertuğrul, Measurement of total, radiative and radiationless (Auger) vacancy transfer probabilities from K to Li sub-shells of Cs, Ba and La, J. Anal. At. Spectrom. 17 (2002) 64–68. https://doi.org/10.1039/b103366m.
[25] M. Ertuğrul, Determination of probabilities of vacancy transfer from the K to the Li subshell using L x-ray production cross-sections, J. Phys. B: At. Mol. Opt. Phys. 36 (2003) 2275–2282. https://doi.org/10.1088/0953-4075/36/11/312.
[26] I. Han, L. Demir, M. Ağbaba, Measurements of L X-ray production cross sections, L subshell fluorescence yields and K to L shell vacancy transfer probabilities, Radiation Physics and Chemistry 76 (2007) 1551–1559. https://doi.org/10.1016/j.radphyschem.2007.04.006.

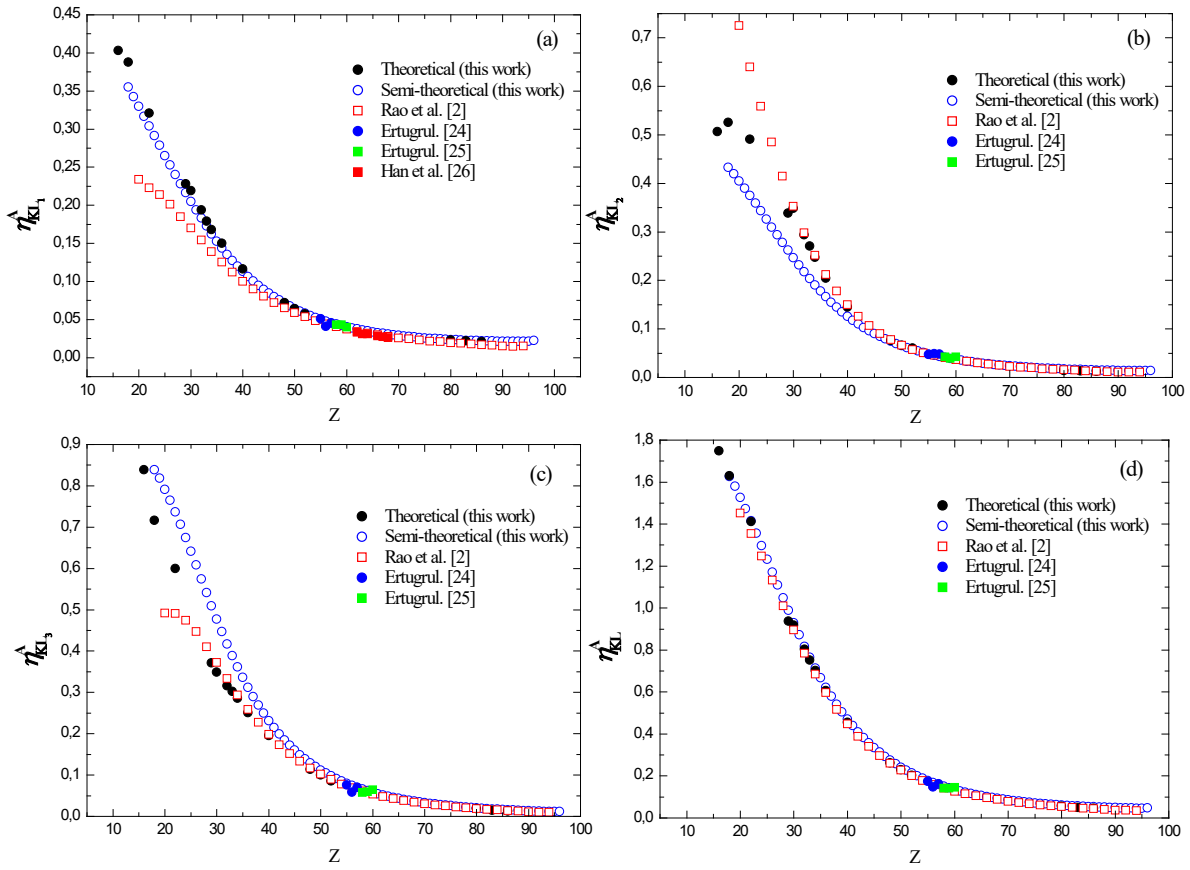
(a)
Theoretical (this work)
Semi-theoretical (this work)
Rao et al. [2]
Ertugrul. [24]
Ertugrul. [25]
Han et al. [26]
$\eta^{\Lambda}_{KL_1}$
Z
(b)
Theoretical (this work)
Semi-theoretical (this work)
Rao et al. [2]
Ertugrul. [24]
Ertugrul. [25]
$\eta^{\Lambda}_{KL_2}$
Z
(c)
Theoretical (this work)
Semi-theoretical (this work)
Rao et al. [2]
Ertugrul. [24]
Ertugrul. [25]
$\eta^{\Lambda}_{KL_3}$
Z
(d)
Theoretical (this work)
Semi-theoretical (this work)
Rao et al. [2]
Ertugrul. [24]
Ertugrul. [25]
η^{Λ}_{KL}
Z

.

Fig .1

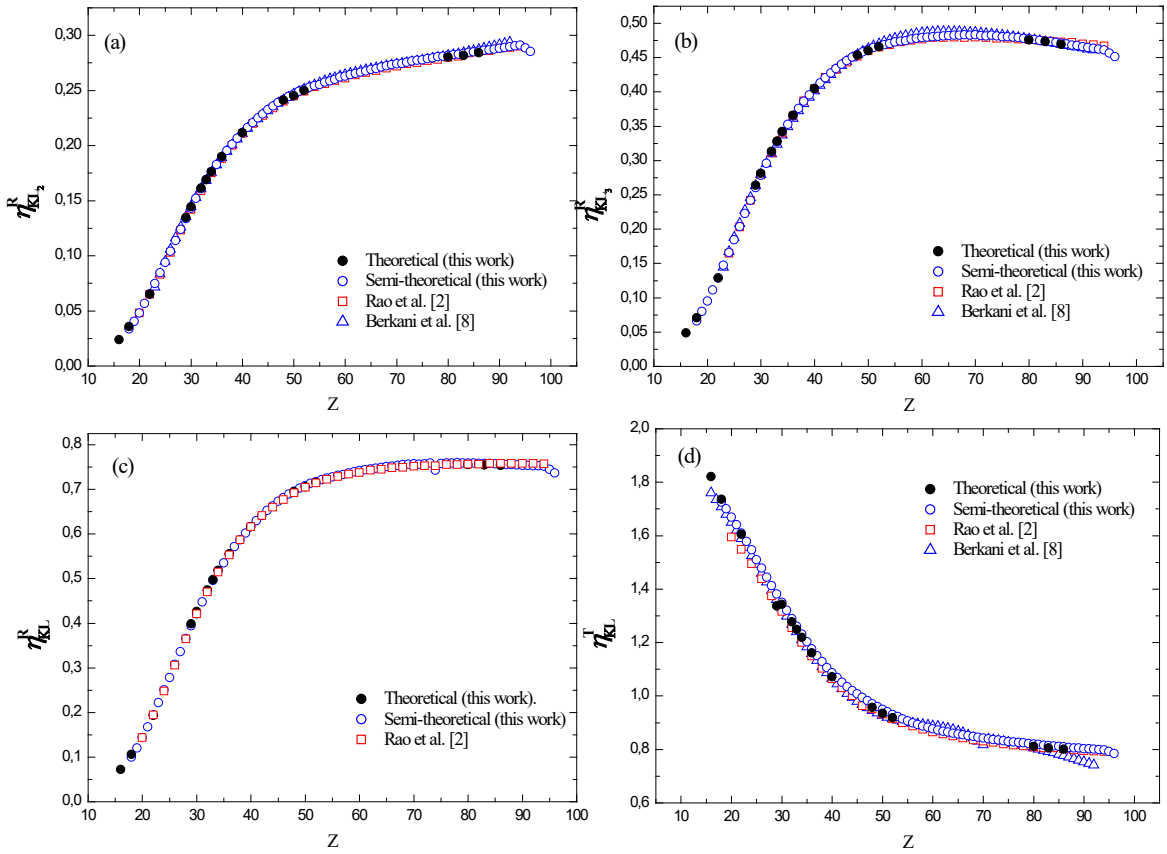
(a)
Theoretical (this work)
Semi-theoretical (this work)
Rao et al. [2]
Berkani et al. [8]
Z
(b)
Theoretical (this work)
Semi-theoretical (this work)
Rao et al. [2]
Berkani et al. [8]
Z
(c)
Theoretical (this work).
Semi-theoretical (this work)
Rao et al. [2]
Z
(d)
Theoretical (this work)
Semi-theoretical (this work)
Rao et al. [2]
Berkani et al. [8]
Z

Fig .2

Table 1. Summary of present theoretical vacancy transfer probabilities from K- to L shell/sub shell.

Z, Symbol	$\eta^{R}_{KL_2}$	$\eta^{R}_{KL_3}$	$\eta^{A}_{KL_1}$	$\eta^{A}_{KL_2}$	$\eta^{A}_{KL_3}$	η^{R}_{KL}	η^{A}_{KL}	η^{T}_{KL}
Z=16, S	0.0238	0.0487	0.403	0.506	0.839	0.0725	1.75	1.82
Z=18, Ar	0.0356	0.0705	0.388	0.526	0.716	0.106	1.63	1.74
Z=22, Ti	0.0651	0.129	0.321	0.491	0.600	0.194	1.41	1.61
Z=29, Cu	0.1355	0.264	0.228	0.339	0.372	0.399	0.938	1.34
Z=30, Zn	0.144	0.282	0.219	0.349	0.349	0.426	0.917	1.34
Z=32, Ge	0.161	0.313	0.194	0.294	0.316	0.475	0.804	1.28
Z=33, As	0.169	0.328	0.179	0.271	0.303	0.497	0.753	1.25
Z=34, Se	0.176	0.342	0.168	0.248	0.286	0.518	0.701	1.22
Z=36, Kr	0.190	0.366	0.150	0.206	0.250	0.556	0.606	1.16
Z=40, Zr	0.212	0.405	0.117	0.145	0.195	0.617	0.456	1.07
Z=48, Cd	0.241	0.454	0.0720	0.0761	0.114	0.695	0.262	0.957
Z=50, Sn	0.245	0.460	0.0642	0.0660	0.100	0.705	0.230	0.936
Z=52, Te	0.250	0.466	0.0571	0.0606	0.0859	0.716	0.204	0.919
Z=80, Hg	0.280	0.476	0.0230	0.0144	0.0181	0.756	0.0555	0.811
Z=83, Bi	0.282	0.473	0.0219	0.0132	0.0150	0.755	0.0501	0.805
Z=86, Rn	0.284	0.470	0.0211	0.0122	0.0131	0.754	0.0464	0.800

Table 2. Summary of fitting coefficients of K-Shell Auger Transition Probabilities (in milliatomic units).

K-Shell Transition	The fitting coefficients according to eq (13) (in ma.u)						Z-group
	A_0	A_1	A_2	A_3	A_4	A_5	
K-L1L1	1.43198	-0.04153	0.00337	4.19268×10^{-7}	-5.61223×10^{-5}	0	$18 \le Z \le 96$
K-L1L2	3.93581	-0.30556	0.0137	-2.25738×10^{-4}	1.49744×10^{-6}	0	$18 \le Z \le 96$
K-L1L3	0.32523	0.21736	-0.0043	4.51691×10^{-5}	-1.45319×10^{-7}	0	$18 \le Z \le 96$
K-L1M1	0.59848	-0.04273	0.00213	-3.11543×10^{-5}	2.05791×10^{-7}	0	$18 \le Z \le 96$
K-L1M2	0.84349	-0.08422	0.00354	-5.54598×10^{-5}	3.51545×10^{-7}	0	$18 \le Z \le 96$
K-L1M3	-0.11958	0.02723	-2.21402×10^{-4}	2.12355×10^{-6}	-5.01441×10^{-10}	0	$18 \le Z \le 96$
K-L1M4	-0.01783	5.5577×10^{-4}	2.60084×10^{-5}	-1.28031×10^{-7}	7.70214×10^{-10}	0	$25 \le Z \le 96$
K-L1M5	-0.10022	0.00514	-3.97778×10^{-5}	1.11781×10^{-7}	0	0	$25 \le Z \le 96$
K-L1N1	0.54686	-0.05241	0.00178	-2.31417×10^{-5}	1.1945×10^{-7}	0	$20 \le Z \le 96$
K-L1N2	0.94729	-0.08196	0.00256	-3.33305×10^{-5}	1.70652×10^{-5}	0	$35 \le Z \le 96$
K-L1N3	-0.63677	0.03139	-4.25662×10^{-4}	2.59799×10^{-6}	-1.52606×10^{-9}	0	$35 \le Z \le 96$
K-L1O1	-2.21039	0.12072	-0.00235	1.90532×10^{-5}	-4.89233×10^{-8}	0	$45 \le Z \le 96$
K-L1O2	-2.97372	0.16031	-0.00308	2.43546×10^{-5}	-6.09806×10^{-8}	0	$50 \le Z \le 96$
K-L1O3	-23.47036	1.57219	-0.04151	5.40547×10^{-4}	-3.47459×10^{-6}	8.84249×10^{-9}	$52 \le Z \le 96$
K-L2L2	-0.02077	0.02443	-4.54547×10^{-4}	4.49399×10^{-6}	-1.4388×10^{-8}	0	$18 \le Z \le 96$
K-L2L3	0.00895	0.58456	-0.01181	1.13848×10^{-4}	-4.04435×10^{-7}	0	$18 \le Z \le 96$
K-L2M1	0.69827	-0.06597	0.00278	-4.42823×10^{-5}	2.83489×10^{-7}	0	$18 \le Z \le 96$
K-L2M2	-0.00828	0.00321	3.80557×10^{-5}	-7.96121×10^{-7}	4.70371×10^{-9}	0	$18 \le Z \le 96$
K-L2M3	-0.10583	0.04377	-8.56342×10^{-6}	-3.62482×10^{-6}	2.47269×10^{-8}	0	$18 \le Z \le 96$
K-L2M4	-6.61×10^{-4}	-0.00155	1.22877×10^{-4}	-1.59124×10^{-6}	7.60034×10^{-9}	0	$25 \le Z \le 96$
K-L2M5	-0.53996	0.03221	-4.97791×10^{-4}	4.24083×10^{-6}	-1.5087×10^{-8}	0	$25 \le Z \le 96$
K-L2N1	0.4126	-0.0409	0.00144	-2.05586×10^{-5}	1.14115×10^{-7}	0	$20 \le Z \le 96$
K-L2N2	-0.07366	0.00298	-1.08516×10^{-5}	-2.18374×10^{-7}	2.01524×10^{-9}	0	$35 \le Z \le 96$
K-L2N3	-1.4038	0.07383	-0.00115	8.21283×10^{-6}	-1.90683×10^{-8}	0	$35 \le Z \le 96$
K-L2N5	-1.32635	0.07172	-0.00141	1.24811×10^{-5}	-4.09879×10^{-8}	0	$45 \le Z \le 96$
K-L2O1	-0.45182	0.01624	-6.27358×10^{-5}	-2.92799×10^{-6}	2.83166×10^{-8}	0	$45 \le Z \le 96$
K-L2O3	-38.63684	2.58226	-0.06799	8.82805×10^{-4}	-5.6544×10^{-6}	1.43197×10^{-8}	$52 \le Z \le 96$
K-L3L3	-0.32028	0.37241	-0.00821	7.84117×10^{-5}	-2.75032×10^{-7}	0	$18 \le Z \le 96$
K-L3M1	-0.07254	0.02704	-3.8052×10^{-4}	3.83249×10^{-6}	-1.00358×10^{-8}	0	$18 \le Z \le 96$
K-L3M2	-0.41516	0.07257	-8.47988×10^{-4}	6.08788×10^{-6}	-1.73959×10^{-8}	0	$18 \le Z \le 96$
K-L3M3	-0.47514	0.08467	-0.00104	6.08612×10^{-6}	-1.09006×10^{-8}	0	$18 \le Z \le 96$
K-L3M4	-0.26356	0.01469	-2.58975×10^{-5}	-1.33083×10^{-6}	7.85299×10^{-9}	0	$25 \le Z \le 96$
K-L3M5	-0.13045	0.00218	3.50586×10^{-4}	-5.75817×10^{-6}	2.55519×10^{-8}	0	$20 \le Z \le 96$
K-L3N1	0.03432	-0.00594	3.27147×10^{-4}	-4.27377×10^{-6}	2.00378×10^{-8}	0	$25 \le Z \le 96$
K-L3N2	-0.61346	0.03057	-3.00891×10^{-4}	1.27078×10^{-6}	0	0	$35 \le Z \le 96$
K-L3N3	-0.85355	0.04171	-4.18297×10^{-4}	9.32657×10^{-7}	6.55145×10^{-9}	0	$35 \le Z \le 96$
K-L3N4	0.20425	-0.01957	5.98936×10^{-4}	-6.77326×10^{-6}	2.67063×10^{-8}	0	$36 \le Z \le 96$
K-L3N5	-1.19165	0.06273	-0.00119	1.01236×10^{-5}	-3.23601×10^{-8}	0	$42 \le Z \le 96$
K-L3O1	-0.04424	0.00218	-3.21004×10^{-5}	2.66389×10^{-7}	0	0	$36 \le Z \le 96$
K-L3O2	-12.74728	0.83614	-0.02144	2.69283×10^{-4}	-1.65381×10^{-6}	3.98278×10^{-9}	$50 \le Z \le 96$
K-L3O3	-40.68767	2.73221	-0.07234	9.45252×10^{-4}	-6.09833×10^{-6}	1.55641×10^{-8}	$52 \le Z \le 96$
K-M1M1	0.04633	-0.00429	2.08446×10^{-4}	-3.03752×10^{-6}	2.05937×10^{-8}	0	$18 \le Z \le 96$
K-M1M2	0.14571	-0.01563	6.46486×10^{-4}	-1.02796×10^{-5}	6.63567×10^{-8}	0	$18 \le Z \le 96$
K-M1M3	-0.00881	0.00165	4.05434×10^{-5}	-4.39626×10^{-7}	2.84052×10^{-9}	0	$18 \le Z \le 96$
K-M1N1	0.08805	-0.00859	2.94186×10^{-4}	-3.86122×10^{-6}	2.08828×10^{-8}	0	$20 \le Z \le 96$
K-M1N2	0.23307	-0.01871	5.51167×10^{-4}	-6.99051×10^{-6}	3.50156×10^{-8}	0	$35 \le Z \le 96$
K-M1N3	0.0041	-0.00156	7.58579×10^{-5}	-9.37727×10^{-7}	4.46148×10^{-9}	0	$35 \le Z \le 96$
K-M2M3	-0.021	0.00266	1.31373×10^{-4}	-1.6546×10^{-6}	6.60704×10^{-9}	0	$18 \le Z \le 96$
K-M2N1	0.07973	-0.00794	2.79061×10^{-4}	-4.00167×10^{-6}	2.27491×10^{-8}	0	$20 \le Z \le 96$
K-M2N3	0.01916	-0.00408	1.80809×10^{-4}	-2.20393×10^{-6}	9.40004×10^{-9}	0	$35 \le Z \le 96$
K-M3M3	-0.01329	0.00163	7.75639×10^{-5}	-1.18043×10^{-6}	5.57046×10^{-9}	0	$18 \le Z \le 96$

K-M3M4	-0.01007	-1.95155×10^{-4}	4.83952×10^{-5}	-6.513×10^{-7}	2.71966×10^{-9}	0	$25 \le Z \le 96$
K-M3M5	-0.06565	0.00369	-4.97969×10^{-5}	4.25113×10^{-7}	-1.64814×10^{-9}	0	$25 \le Z \le 96$
K-M3N1	0.03414	-0.00326	1.12001×10^{-4}	-1.25857×10^{-6}	5.43176×10^{-9}	0	$20 \le Z \le 96$
K-M3N2	-0.0207	-0.00174	1.36767×10^{-4}	-1.86085×10^{-6}	8.54232×10^{-9}	0	$35 \le Z \le 96$
K-M3M3	0.05661	-0.00613	2.19811×10^{-4}	-2.50024×10^{-6}	1.02387×10^{-8}	0	$35 \le Z \le 96$

Table 3. Summary of semi-theoretical vacancy transfer probabilities from K- to L shell/subsh ell for elements within the atomic range of $18 \leq Z \leq 96$.

Z, Symbol	$\eta^{R}_{KL_2}$	$\eta^{R}_{KL_3}$	$\eta^{A}_{KL_1}$	$\eta^{A}_{KL_2}$	$\eta^{A}_{KL_3}$	η^{R}_{KL}	η^{A}_{KL}	η^{T}_{KL}
Z=18, Ar	0.0336	0.0664	0.3553	0.4326	0.8388	0.1000	1.6267	1.7267
Z=19, K	0.0406	0.0802	0.3422	0.4194	0.8179	0.1208	1.5795	1.7003
Z=20, Ca	0.0482	0.0950	0.3297	0.4049	0.7914	0.1432	1.5261	1.6693
Z=21, Sc	0.0566	0.1115	0.3168	0.3903	0.7653	0.1681	1.4723	1.6404
Z=22, Ti	0.0655	0.1288	0.3039	0.3749	0.7368	0.1943	1.4155	1.6099
Z=23, V	0.0748	0.1471	0.2911	0.3591	0.7062	0.2219	1.3564	1.5783
Z=24, Cr	0.0845	0.1660	0.2785	0.3432	0.6746	0.2505	1.2962	1.5468
Z=25, Mn	0.0939	0.1842	0.2649	0.3259	0.6413	0.2782	1.2321	1.5103
Z=26, Fe	0.1040	0.2035	0.2526	0.3100	0.6083	0.3075	1.1709	1.4784
Z=27, Co	0.1139	0.2226	0.2401	0.2938	0.5747	0.3365	1.1086	1.4450
Z=28, Ni	0.1237	0.2419	0.2281	0.2779	0.5416	0.3656	1.0476	1.4132
Z=29, Cu	0.1335	0.2606	0.2164	0.2623	0.5093	0.3942	0.9881	1.3822
Z=30, Zn	0.1430	0.2785	0.2049	0.2471	0.4776	0.4214	0.9295	1.3510
Z=31, Ga	0.1521	0.2956	0.1938	0.2321	0.4467	0.4477	0.8726	1.3203
Z=32, Ge	0.1607	0.3117	0.1830	0.2177	0.4170	0.4724	0.8177	1.2901
Z=33, As	0.1689	0.3274	0.1725	0.2038	0.3883	0.4963	0.7646	1.2608
Z=34, Se	0.1764	0.3414	0.1624	0.1906	0.3611	0.5178	0.7141	1.2319
Z=35, Br	0.1827	0.3526	0.1529	0.1780	0.3365	0.5354	0.6674	1.2028
Z=36, Kr	0.1892	0.3647	0.1438	0.1662	0.3124	0.5538	0.6224	1.1763
Z=37, Rb	0.1954	0.3759	0.1353	0.1552	0.2899	0.5713	0.5804	1.1517
Z=38, Sr	0.2011	0.3862	0.1274	0.1448	0.2690	0.5872	0.5412	1.1284
Z=39, Y	0.2066	0.3959	0.1199	0.1352	0.2495	0.6024	0.5046	1.1070
Z=40, Zr	0.2116	0.4049	0.1129	0.1262	0.2315	0.6166	0.4707	1.0872
Z=41, Nb	0.2164	0.4132	0.1064	0.1179	0.2149	0.6296	0.4392	1.0687
Z=42, Mo	0.2208	0.4207	0.1003	0.1101	0.1994	0.6416	0.4097	1.0513
Z=43, Tc	0.2249	0.4277	0.0946	0.1028	0.1851	0.6526	0.3826	1.0351
Z=44, Ru	0.2287	0.4340	0.0892	0.0961	0.1719	0.6626	0.3573	1.0199
Z=45, Rh	0.2326	0.4404	0.0844	0.0901	0.1601	0.6730	0.3346	1.0076
Z=46, Pd	0.2359	0.4456	0.0798	0.0844	0.1488	0.6815	0.3130	0.9945
Z=47, Ag	0.2390	0.4505	0.0755	0.0791	0.1386	0.6895	0.2932	0.9827
Z=48, Cd	0.2417	0.4542	0.0715	0.0741	0.1289	0.6960	0.2746	0.9706
Z=49, In	0.2446	0.4584	0.0678	0.0696	0.1202	0.7029	0.2576	0.9606
Z=50, Sn	0.2467	0.4615	0.0643	0.0653	0.1120	0.7082	0.2417	0.9498
Z=51, Sb	0.2490	0.4649	0.0611	0.0614	0.1046	0.7139	0.2271	0.9410
Z=52, Te	0.2508	0.4664	0.0581	0.0578	0.0977	0.7173	0.2135	0.9308
Z=53, I	0.2527	0.4688	0.0553	0.0545	0.0913	0.7215	0.2010	0.9225
Z=54, Xe	0.2543	0.4706	0.0526	0.0513	0.0854	0.7248	0.1894	0.9142
Z=55, Cs	0.2554	0.4726	0.0502	0.0484	0.0799	0.7281	0.1785	0.9066
Z=56, Ba	0.2574	0.4737	0.0480	0.0458	0.0748	0.7311	0.1686	0.8997
Z=57, La	0.2587	0.4747	0.0458	0.0433	0.0701	0.7334	0.1593	0.8927
Z=58, Ce	0.2600	0.4767	0.0439	0.0410	0.0659	0.7367	0.1509	0.8875
Z=59, Pr	0.2620	0.4779	0.0421	0.0389	0.0619	0.7398	0.1430	0.8829
Z=60, Nd	0.2628	0.4789	0.0405	0.0370	0.0583	0.7417	0.1357	0.8774
Z=61, Pm	0.2644	0.4797	0.0389	0.0352	0.0549	0.7441	0.1289	0.8730
Z=62, Sm	0.2654	0.4806	0.0375	0.0335	0.0517	0.7460	0.1226	0.8686

Z=63, Eu	0.2666	0.4812	0.0361	0.0319	0.0487	0.7478	0.1168	0.8646
Z=64, Gd	0.2676	0.4813	0.0349	0.0304	0.0460	0.7490	0.1113	0.8602
Z=65, Tb	0.2689	0.4823	0.0337	0.0291	0.0435	0.7512	0.1063	0.8575
Z=66, Dy	0.2699	0.4824	0.0327	0.0279	0.0411	0.7523	0.1016	0.8540
Z=67, Ho	0.2712	0.4828	0.0317	0.0267	0.0389	0.7540	0.0973	0.8512
Z=68, Er	0.2722	0.4830	0.0307	0.0256	0.0369	0.7552	0.0932	0.8485
Z=69, Tm	0.2732	0.4828	0.0299	0.0246	0.0349	0.7560	0.0894	0.8455
Z=70, Yb	0.2742	0.4830	0.0291	0.0237	0.0332	0.7572	0.0860	0.8431
Z=71, Lu	0.2746	0.4821	0.0283	0.0228	0.0315	0.7567	0.0826	0.8393
Z=72, Hf	0.2754	0.4817	0.0276	0.0220	0.0299	0.7572	0.0795	0.8367
Z=73, Ta	0.2767	0.4825	0.0270	0.0213	0.0285	0.7592	0.0768	0.8360
Z=74, W	0.2772	0.4814	0.0264	0.0206	0.0271	0.7586	0.0741	0.8327
Z=75, Re	0.2776	0.4803	0.0258	0.0199	0.0258	0.7579	0.0715	0.8294
Z=76, Os	0.2787	0.4801	0.0253	0.0193	0.0246	0.7589	0.0693	0.8281
Z=77, Ir	0.2796	0.4798	0.0249	0.0188	0.0235	0.7594	0.0671	0.8265
Z=78, Pt	0.2805	0.4793	0.0245	0.0183	0.0224	0.7599	0.0652	0.8250
Z=79, Au	0.2809	0.4778	0.0240	0.0178	0.0214	0.7587	0.0632	0.8219
Z=80, Hg	0.2815	0.4772	0.0237	0.0173	0.0204	0.7587	0.0615	0.8201
Z=81, Tl	0.2823	0.4764	0.0234	0.0169	0.0196	0.7587	0.0598	0.8186
Z=82, Pb	0.2828	0.4749	0.0230	0.0165	0.0187	0.7577	0.0582	0.8160
Z=83, Bi	0.2836	0.4742	0.0227	0.0162	0.0179	0.7579	0.0568	0.8147
Z=84, Po	0.2845	0.4735	0.0225	0.0159	0.0172	0.7579	0.0555	0.8135
Z=85, At	0.2849	0.4721	0.0223	0.0155	0.0165	0.7570	0.0543	0.8113
Z=86, Rn	0.2855	0.4708	0.0220	0.0153	0.0158	0.7563	0.0531	0.8093
Z=87, Fr	0.2862	0.4696	0.0218	0.0150	0.0152	0.7557	0.0520	0.8077
Z=88, Ra	0.2868	0.4683	0.0217	0.0147	0.0146	0.7551	0.0510	0.8061
Z=89, Ac	0.2876	0.4673	0.0215	0.0145	0.0140	0.7549	0.0500	0.8049
Z=90, Th	0.2881	0.4658	0.0214	0.0143	0.0134	0.7539	0.0491	0.8030
Z=91, Pa	0.2889	0.4646	0.0216	0.0141	0.0129	0.7536	0.0487	0.8023
Z=92, U	0.2896	0.4633	0.0215	0.0140	0.0125	0.7529	0.0479	0.8008
Z=93, Np	0.2904	0.4621	0.0214	0.0138	0.0120	0.7525	0.0472	0.7997
Z=94, Pu	0.2912	0.4609	0.0213	0.0137	0.0116	0.7521	0.0466	0.7987
Z=95, Am	0.2884	0.4564	0.0212	0.0140	0.0115	0.7448	0.0467	0.7915
Z=96, Cm	0.2852	0.4515	0.0223	0.0143	0.0114	0.7367	0.0480	0.7847